Theory of Photoionization-Induced Blueshift of Ultrashort Solitons in Gas-Filled Hollow-Core Photonic Crystal Fibers

Mohammed F. Saleh,[1] Wonkeun Chang,[1] Philipp Hölzer,[1] Alexander Nazarkin,[1] John C. Travers,[1] Nicolas Y. Joly,[1,2] Philip St. J. Russell,[1,2] and Fabio Biancalana[1]

[1]*Max Planck Institute for the Science of Light, Günther-Scharowsky Strasse 1, 91058 Erlangen, Germany*
[2]*Department of Physics, University of Erlangen-Nuremberg, 91054 Erlangen, Germany*

(Received 27 June 2011; published 7 November 2011)

We show theoretically that the photoionization process in a hollow-core photonic crystal fiber filled with a Raman-inactive noble gas leads to a constant acceleration of solitons in the time domain with a continuous shift to higher frequencies, limited only by ionization loss. This phenomenon is opposite to the well-known Raman self-frequency redshift of solitons in solid-core glass fibers. We also predict the existence of unconventional long-range nonlocal soliton interactions leading to spectral and temporal soliton clustering. Furthermore, if the core is filled with a Raman-active molecular gas, spectral transformations between redshifted, blueshifted, and stabilized solitons can take place in the same fiber.

DOI: 10.1103/PhysRevLett.107.203902 PACS numbers: 42.65.Tg, 05.45.Yv, 32.80.Fb

Introduction.—Hollow-core (HC) photonic crystal fibers (PCFs) [1] based on a kagome-lattice cladding have recently been shown to be very interesting for the investigation of broadband light-matter interactions between intense optical pulses and gaseous media. The fibers typically show transmission bands covering the visible and near-IR parts of the spectrum with relatively low loss and low group velocity dispersion (GVD), absence of surface modes, and high confinement of light in the core. Filled with a noble gas, they have recently been used in high-harmonic and efficient deep UV generation from femtosecond pump pulses at 800 nm [2–4]. It has been previously shown that the Raman threshold can be drastically reduced in a HC PCF filled with a Raman-active gas (such as H_2) [5]. The system can be used for detailed experimental studies of, e.g., self-similar solutions of the sine-Gordon equation [6], backward stimulated Raman scattering [5,7].

The concept of soliton self-frequency blue-shift has been introduced and predicted in Ref. [8]. Soliton blueshift has been recently observed in tapered solid-core photonic crystal fibers [9] as a result of the variation of the zero-dispersion wavelength along the fiber. In conventional band-gap-guiding gas-filled HC PCFs, which have narrow bands of transmission, a limited ionization-induced blueshift of guided ultrashort pulses has been reported [10,11]. Very recently, ultrafast nonlinear dynamics in the ionization regime has been studied experimentally in Ar-filled kagome-style HC PCF [12] (a detailed account of these experiments is available in a parallel submission [13]). The reasons for the success of kagome HC PCF in these applications are (i) a GVD that is remarkably small ($|\beta_2| < 10$ fs^2/cm $\equiv 1$ ps^2/km from 400 to 1000 nm) in comparison to solid-core fibers [Fig. 1(a)] [3,13] and (ii) the gas and waveguide contributions to the GVD can be balanced by varying the pressure, unlike in large-bore capillary-based systems where the normal dispersion of the gas dominates over the waveguide dispersion [4].

Photoionization in gases is traditionally modeled by using the full electric field of the pulse [14]. In this Letter, we first develop a new model to study pulse propagation in gas-filled HC PCFs in terms of the complex *envelope* of the pulse. Using this model, we show analytically for the first time that intrapulse photoionization leads to (i) a soliton self-frequency blueshift; (ii) long-range "nonlocal" soliton correlations and clustering; and (iii) spectral transformations of redshifted, blueshifted,

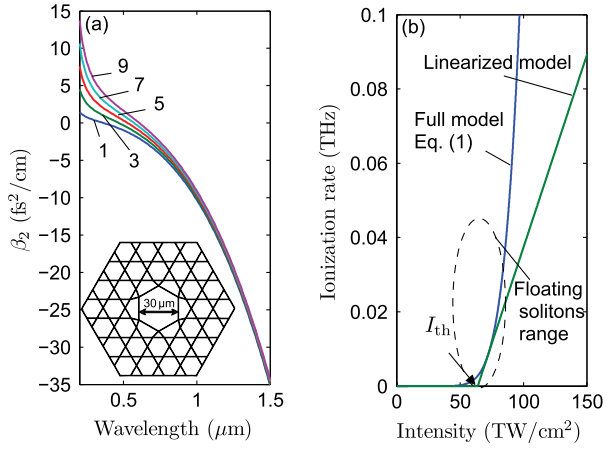

FIG. 1 (color online). (a) GVD of an Ar-filled HC PCF for gas pressures between 1 and 9 bar (calculated from Ref. [30]). All subsequent calculations in this Letter assume 5 bar pressure. Inset: Cross section of a broadband-guiding HC PCF with a kagome-lattice cladding and a core diameter 30 μm. Typical experimental transmission losses for the fundamental mode are 1 dB/m at 800 nm. (b) Comparison of the dependence of the Ar ionization rate on the pulse intensity using the full model of Eq. (1) and the linearized model.

and stabilized solitons in Raman-active gas-filled HC PCFs.

Governing equations.—Photoionization can take place by either tunneling or multiphoton processes. These regimes are characterized by the Keldysh parameter p_K [14,15]. In the tunneling regime ($p_K \ll 1$) the time-averaged ionization rate $\mathcal{W}(I)$ is given by [16,17]

$$\mathcal{W}(I) = d(I_H/I)^{1/4} \exp[-b(I_H/I)^{1/2}], \quad (1)$$

where $d \equiv 4\delta_0[3/\pi]^{1/2}[U_I/U_H]^{7/4}$, $b \equiv 2/3[U_I/U_H]^{3/2}$, $\delta_0 = 4.1 \times 10^{16}$ Hz is the characteristic atomic frequency, U_I is the ionization energy of the gas (~ 15.76 eV for argon), $U_H \approx 13.6$ eV is the ionization energy of hydrogen, $I_H = 3.6 \times 10^{16}$ W/cm^2, and I is the laser pulse intensity. For values of I in the range of 100 TW/cm^2, the Keldysh parameter is $p_K \lesssim 1$ for noble gases. However, experiments show that tunneling models provide excellent agreement with the experimental measurements even for $p_K \approx 1$ [18,19]. As shown in Fig. 1(b), Eq. (1) predicts an ionization rate that is exponential-like for pulse intensities above a threshold value. Loss due to absorption of photons in the plasma is *proportional* to the ionization rate. Hence, any pulse with $I \gg I_{th}$ will have its intensity strongly driven back to near the threshold value, resulting in drastically reduced the ionization loss. This allows us to use the first-order Taylor series to *linearize* the tunneling model just above $I = I_{th}$, where the optical pulses can survive for a relatively long time without appreciable attenuation. Expanding Eq. (1) in its linear regime around an arbitrary point $a = I_a/I_H$ results in $\mathcal{W} \approx \tilde{\sigma}\Delta I\Theta(\Delta I)$, where $\Delta I \equiv I - I_{th}$, $\tilde{\sigma} = de^{-x}(2x-1)/[4a^{5/4}I_H]$, $I_{th} = aI_H(2x-5)/(2x-1)$ is the threshold intensity, $x = b/\sqrt{a}$, and a is chosen to reproduce the physically observed threshold intensity in the fiber of Fig. 1(a), $a \cong 2 \times 10^{-3}$. The purpose of the Heaviside function Θ is to set the ionization rate to zero below the threshold intensity. As shown in Fig. 1(b), the linearized model underestimates the ionization rate then the ionization loss, in comparison to the full model. This yields to a similar qualitative behavior between the two models even for $I > I_{th}$, since the ionization rate and the ionization loss are the key factors in the photoionization process.

One can prove from first principles that propagation of light in a HC PCF filled with an ionized Raman-active gas can be then described by the following coupled equations:

$$\left[i\partial_z + \hat{D}(i\partial_t) + \gamma_K R(t) \otimes |\Psi(t)|^2 - \frac{\omega_p^2}{2k_0c^2} + i\alpha\right]\Psi = 0,$$
$$\partial_t n_e = [\tilde{\sigma}/A_{eff}][n_T - n_e]\Delta|\Psi|^2\Theta(\Delta|\Psi|^2), \quad (2)$$

where $\Psi(z, t)$ is the electric field *envelope*, z is the longitudinal coordinate along the fiber, t is the time in a reference frame moving with the pulse group velocity, $\hat{D}(i\partial_t) \equiv \sum_{m\geq 2}\beta_m(i\partial_t)^m/m!$ is the full dispersion operator, β_m is the mth order dispersion coefficient calculated at an arbitrary reference frequency ω_0, γ_K is the Kerr nonlinear coefficient of the gas, $R(t) = (1-\rho)\delta(t) + \rho h(t)$ is the normalized Kerr and Raman response function of the gas, $\delta(t)$ is the Dirac delta function, ρ is the relative strength of the noninstantaneous Raman nonlinearity, $h(t)$ is the causal Raman response function of the gas [10,20], the symbol $\otimes$ denotes the time convolution, c is the speed of light, $k_0 = \omega_0/c$, ω_0 is the pulse central frequency, $\omega_p = [e^2n_e/(\epsilon_0 m_e)]^{1/2}$ is the plasma frequency associated with an electron density $n_e(t)$, e and m_e are the electron charge and mass, respectively, and ϵ_0 is the vacuum permittivity, $\alpha = \alpha_1 + \alpha_2$ is the total loss coefficient, α_1 is the fiber loss, $\alpha_2 = \frac{A_{eff}U_I}{2|\Psi|^2}\partial_t n_e$ is the ionization-induced loss term, A_{eff} is the effective mode area, $\Delta|\Psi|^2 = |\Psi|^2 - |\Psi|^2_{th}$, $|\Psi|^2 = IA_{eff}$, $|\Psi|^2_{th} = I_{th}A_{eff}$, and n_T is the total number density of ionizable atoms in the fiber, associated with the maximum plasma frequency $\omega_T \equiv [e^2n_T/(\epsilon_0 m_e)]^{1/2}$. In these coupled equations, the recombination process is neglected since the pulse duration (of the order of tens of femtoseconds) is always shorter than the recombination time [21]. If $|\Psi|^2$ is measured in watts, $\tilde{\sigma}/cA_{eff} \equiv \gamma_I$ has the dimensions of $W^{-1}m^{-1}$. This is the nonlinearity associated with the plasma formation in the fiber. According to recent experimental measurements [22], γ_K shows a linear dependence on the gas pressure. These coupled equations (2) are the first contribution of this Letter. The validity of Eqs. (2) has been verified by using a more complete ionization model based on the unidirectional wave equation [23].

Perturbation theory for floating pulses.—In order to extract useful analytical information from Eqs. (2), further simplifications are necessary. For pulses with maximum intensities just above the ionization threshold (which we dub *floating* pulses, a new concept introduced in this Letter for the first time), the ionization loss is not large and can be neglected as a first approximation. For such pulses, only a small portion of energy above the threshold intensity contributes to the creation of free electrons. Furthermore, for floating pulses one can remove the Θ function from the equations, provided that the cross section $\tilde{\sigma}$ is replaced by a properly reduced $\tilde{\sigma}'$ that takes into account the overestimation of the ionization rate [24]. Introducing the following rescalings and redefinitions: $\xi \equiv z/z_0$, $\tau \equiv t/t_0$, $\Psi_0 \equiv [\gamma_K z_0]^{-1/2}$, $\psi \equiv \Psi/\Psi_0$, $r(\tau) \equiv R(t)t_0$, $\phi \equiv \frac{1}{2}k_0z_0[\omega_p/\omega_0]^2$, $\phi_T \equiv \frac{1}{2}k_0z_0[\omega_T/\omega_0]^2$, and $\sigma \equiv \tilde{\sigma}'t_0/[A_{eff}\gamma_K z_0]$, where $z_0 \equiv t_0^2/|\beta_2(\omega_0)|$ is the second-order dispersion length at the reference frequency ω_0 and t_0 is the input pulse duration [20]. Hence, the two coupled equations for floating pulses can be replaced by

$$[i\partial_\xi + \hat{D}(i\partial_\tau) + r(\tau) \otimes |\psi(\tau)|^2 - \phi]\psi = 0,$$
$$\partial_\tau\phi = \sigma(\phi_T - \phi)|\psi|^2. \quad (3)$$

The total number of photons is conserved in this set of coupled equations—in contrast to Eqs. (2)—since losses are neglected for floating pulses.

The effect of the Raman and ionization perturbations on the soliton dynamics in HC PCFs can be studied by using Eqs. (3). The second equation can be solved analytically, $\phi(\tau) = \phi_T\{1 - e^{-\sigma\int_{-\infty}^{\tau}|\psi(\tau')|^2 d\tau'}\}$, with the initial condition $\phi(-\infty) = 0$, corresponding to the absence of any plasma before the pulse arrives. For a small ionization cross section, $\phi(\tau) \simeq \eta\int_{-\infty}^{\tau}|\psi(\tau')|^2 d\tau'$, where $\eta \equiv \sigma\phi_T$. Moreover, in the long-pulse limit $|\psi(\tau - \tau')|^2 \simeq |\psi(\tau)|^2 - \tau'\partial_\tau|\psi(\tau)|^2$ [20]. This allows the two coupled equations to be reduced to a single partial integro-differential equation:

$$i\partial_\xi\psi + \hat{D}(i\partial_\tau)\psi + |\psi|^2\psi - \tau_R\psi\partial_\tau|\psi|^2 - \eta\psi\int_{-\infty}^{\tau}|\psi|^2 d\tau' = 0, \quad (4)$$

where $\tau_R \equiv \int_0^\infty \tau' r(\tau') d\tau'$. This equation shows clearly that the effect of ionization is exactly opposite to that of the Raman effect: The fourth term in Eq. (4) involves a *derivative* of the field intensity, while the fifth term involves an *integral* on the same quantity. One can then conjecture that the last term will lead to a soliton self-frequency blueshift due to ionization, instead of a redshift due to Raman self-scattering [25–27]. To prove this statement, we use the perturbation theory described in Ref. [20]. First, the soliton functional shape is assumed to be unchanged during the action of the perturbations induced by the Raman effect and the photoionization process (this must be verified *a posteriori*): $\psi_S(\xi,\tau) = A_0\mathrm{sech}\{A_0[\tau - \tau_p(\xi)]\}e^{-i\delta(\xi)\tau}$, with $\tau_p(\xi)$ is the temporal location of the soliton peak and $\delta(\xi)$ is the self-frequency shift. When this ansatz is inserted into Eq. (4), simple ordinary differential equations can be obtained for both $\delta(\xi)$ and $\tau_p(\xi)$, results in $\delta(\xi) = \delta_{\mathrm{Raman}}(\xi) + \delta_{\mathrm{ion}}(\xi) = -g\xi$, $\tau_p(\xi) = g\xi^2/2$, and $g = g_{\mathrm{red}} + g_{\mathrm{blue}}$, where $g_{\mathrm{red}} = +(8/15)\tau_R A_0^4$ and $g_{\mathrm{blue}} = -(2/3)\eta A_0^2$. Note that g can be positive, negative, or even zero, depending on the value of η, τ_R, and A_0. By using the exact solution for $\phi(\tau)$ given previously, one obtains the more precise rate $g'_{\mathrm{blue}} = \sigma^{-2}A_0^{-1}\phi_T[(1 - \sigma A_0) - (1 + \sigma A_0)\exp(-2\sigma A_0)]$, which tends to g_{blue} for small values of σ but starts to differ considerably from it for $A_0 > \sigma^{-1}$. The above solution clearly shows that, in the range of validity of perturbation theory (i.e., for floating solitons), *photoionization leads to a soliton self-frequency blueshift*. This blueshift is accompanied by a constant acceleration of the pulse in the time domain—opposite to the Raman effect, which produces pulse deceleration [26]. This blueshift (distinct from the effects discussed in Refs. [8,9]) is limited only by ionization loss, which slowly decreases the pulse intensity until it falls below the threshold value.

In the presence of ionization-induced losses above the threshold intensity, Eqs. (2) must be numerically solved to study the full dynamics of floating pulses. Figures 2(a) and 2(b) show the temporal and spectral evolution of a high-order input soliton, closely following the results reported in the companion experimental paper [13]. When the intensity of the energetic pulse exceeds the threshold value as a result of self-compression, a fundamental soliton is ejected from the main pulse and continues to blueshift until ionization loss reduces its amplitude below the threshold value. At longer distances, another compression occurs and a second soliton is generated. The use of a kagome-style HC PCF is essential to observe the soliton blueshift, since conventional photonic-band-gap fibers have much stronger dispersion variations, which would quickly destabilize any possible solitary wave as in Refs. [10,11].

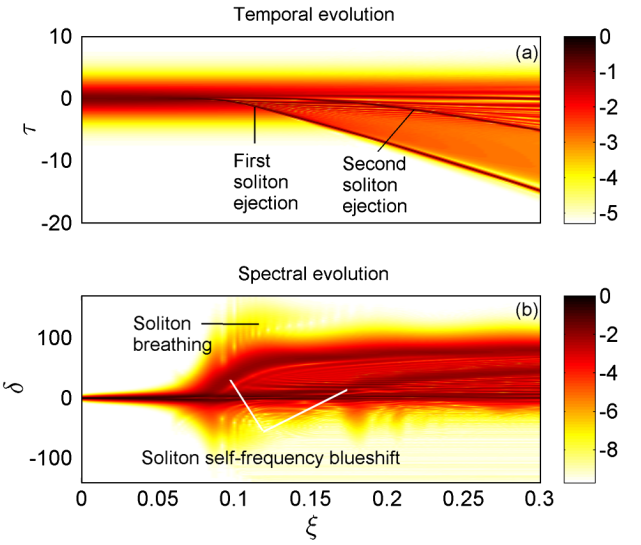

FIG. 2 (color online). Temporal (a) and spectral (b) evolution of an energetic pulse propagating in an Ar-filled HC PCF. The temporal profile of the input pulse is $N\mathrm{sech}\tau$, with $N = 8$. The panels show the ejection of two fundamental solitons that continuously blueshift until ionization loss reduces their intensities below the threshold value. Contour plots in this Letter are given in a logarithmic scale.

Long-range nonlocal soliton forces and clustering.—An interesting and unexpected interaction occurs between two solitons when their temporal separation is shorter than the recombination time, due to the nonvanishing electron density tail. Using the exact formula for the ionization field $\phi(t)$, one can see that a leading soliton with amplitude A_0 can slow down the acceleration of a trailing soliton by an exponential factor $\exp(-2\sigma A_0)$. The reason is that the ionization field $\phi(t)$, created by the first soliton, decays at a relatively slow rate. This establishes a unique nonlocal interaction between this soliton and other temporally distant solitons.

Figures 3(a) and 3(b) show the output temporal and spectral dependence of a pulse $N\mathrm{sech}\tau$ on the soliton order N. In the presence of ionization loss, when the intensity of the leading soliton decreases to the threshold value,

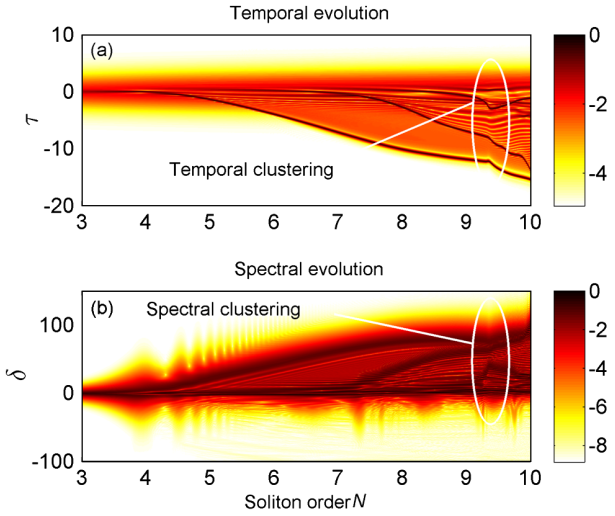

FIG. 3 (color online). Temporal (a) and spectral (b) outputs of an energetic pulse $N\mathrm{sech}\tau$ after propagating inside an Ar-filled HC PCF with length $\xi = 1/4$ versus the soliton order N. Temporal and spectral clustering occur at $N = 9.2$ due to the long-range ''nonlocal'' soliton interactions described in the text.

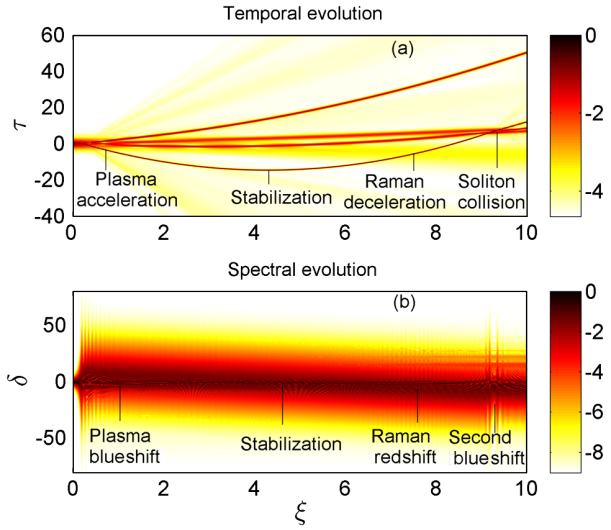

FIG. 4 (color online). Temporal (a) and spectral (b) evolution of an energetic pulse propagates in a HC PCF filled with argon and air. The temporal profile of the input pulse is $N\mathrm{sech}\tau$, with $N = 4$. Soliton temporal and spectral trajectories show an initial acceleration and blueshift due to plasma formation, an intermediate stabilization below-threshold intensity, and finally a deceleration and redshift due to the Raman effect. Near the fiber end, a second blueshift event takes place due to a soliton collision, generating a second surge of ionized plasma.

i.e., the blueshifting process ceases, the trailing soliton will recover its expected blueshift. The reason is the disappearance of the exponential decaying factor at that particular point. Also, there is a maximum frequency attained by each soliton that depends on the initial soliton intensity. These interactions may lead, at some ''magic'' input energy, to clustering two or more distinct solitons in both temporal and spectral domains, as shown in Figs. 3(a) and 3(b).

Soliton spectral transformations.—Interestingly, this perturbation theory for floating solitons predicts the formation of spectrally stabilized solitons in Raman-active gases due to the different signs and A_0 dependence of the Raman and photoionization shifts, $g_{\mathrm{red}} \propto A_0^4$ (a well-known result [20]) and $g_{\mathrm{blue}} \propto -A_0^2$ (reported for the first time in this Letter), respectively. If one launches a sufficiently energetic pulse into the fiber, soliton fission takes place, independent of the particular perturbation applied [28,29]. This generates a train of fundamental solitons with progressively decreasing peak amplitudes.

The temporal and spectral evolution of such a pulse when it propagates in a mixture of argon and air (Raman-active) is depicted in Figs. 4(a) and 4(b). After the fission process, solitons with intensities less than the threshold intensity are redshifted by the undisturbed Raman process. However, solitons possessing intensities above the threshold value are influenced simultaneously by both the photoionization and the Raman effects. Depending on their initial intensities, these solitons can be *initially* blueshifted, redshifted, or stabilized. The Raman self-frequency redshift will be more pronounced than the ionization self-frequency blueshift for floating solitons possessing initially larger amplitudes ($A_j > A_{\mathrm{cr}}$), where A_{cr} is a critical amplitude. However, for less intense floating solitons ($A_j < A_{\mathrm{cr}}$) it may happen that exactly the opposite phenomenon occurs; i.e., the blueshift will dominate. The critical intensity can be estimated from the equation $g_{\mathrm{red}} + g_{\mathrm{blue}} = 0$, giving $A_{\mathrm{cr}}^2 = 5\eta/(4\tau_{\mathrm{R}})$. When the ionization loss arrests the photoionization process, the initially blueshifted solitons start to reverse their self-frequency shift towards the red. At a certain point, these solitons can become frequency-stabilized over a short distance. This may result in multiple collisions between floating solitons if their temporal trajectories intersect. When the instantaneous intensity exceeds the threshold value upon collision, a second blueshift event may occur.

Conclusions.—A direct photoionization process can act on solitons by constantly blueshifting their central frequencies representing the exact counterpart of the Raman self-frequency redshift when the intensity of solitons is slightly above the photoionization threshold. This spectral transformation is limited by the ionization loss that restricts the pulse intensity to the threshold value, hence arresting the soliton blueshift. The new theoretical model, presented by Eqs. (2), is suitable for analytical manipulations and has led us to predict a number of new phenomena such as long-range nonlocal correlation forces and spectral transformation between red- and blueshift in Raman-active gases. The results reveal new physics and offer novel opportunities for the manipulation and control of the soliton dynamics inside these versatile optical waveguides.

[1] P. St. J. Russell, Science **299**, 358 (2003).

[2] O. H. Heckl, C. R. E. Baer, C. Kränkel, S. V. Marchese, F. Schapper, M. Holler, T. Südmeyer, J. S. Robinson, J. W. G. Tisch, F. Couny, P. Light, F. Benabid, and U. Keller, Appl. Phys. B **97**, 369 (2009).

[3] N. Y. Joly, J. Nold, W. Chang, P. Hölzer, A. Nazarkin, G. K. L. Wong, F. Biancalana, and P. St. J. Russell, Phys. Rev. Lett. **106**, 203901 (2011).

[4] J. Nold, P. Hölzer, N. Y. Joly, G. K. L. Wong, A. Nazarkin, A. Podlipensky, M. Scharrer, and P. St. J. Russell, Opt. Lett. **35**, 2922 (2010).

[5] F. Benabid, J. C. Knight, G. Antonopoulos, and P. St. J. Russell, Science **298**, 399 (2002).

[6] A. Nazarkin, A. Abdolvand, A. V. Chugreev, and P. St. J. Russell, Phys. Rev. Lett. **105**, 173902 (2010).

[7] A. Abdolvand, A. Nazarkin, A. V. Chugreev, C. F. Kaminski, and P. St. J. Russell, Phys. Rev. Lett. **103**, 183902 (2009).

[8] V. N. Serkin and V. A. Vysloukh, in *Nonlinear Guided Wave Phenomena*, Technical Digest Vol. 14 (Optical Society of America, Washington, DC, 1993), pp. 236–239.

[9] S. P. Stark, A. Podlipensky, and P. St. J. Russell, Phys. Rev. Lett. **106**, 083903 (2011).

[10] E. E. Serebryannikov and A. M. Zheltikov, Phys. Rev. A **76**, 013820 (2007).

[11] A. B. Fedotov, E. E. Serebryannikov, and A. M. Zheltikov, Phys. Rev. A **76**, 053811 (2007).

[12] P. Hölzer, W. Chang, J. Nold, J. C. Travers, A. Nazarkin, N. Y. Joly, and P. St. J. Russell, in *Proceedings of the Conference on Lasers and Electro-Optics (CLEO), Baltimore, MD, 2011* (Optical Society of America, Washington, DC, 2011), CMJ3.

[13] P. Hölzer, W. Chang, J. C. Travers, A. Nazarkin, J. Nold, N. Y. Joly, M. F. Saleh, F. Biancalana, and P. St. J. Russell, preceding Letter, Phys. Rev. Lett. **107**, 203901 (2011).

[14] M. Geissler, G. Tempea, A. Scrinzi, M. Schnürer, F. Krausz, and T. Brabec, Phys. Rev. Lett. **83**, 2930 (1999).

[15] M. Wegener, *Extreme Nonlinear Optics* (Springer-Verlag, Berlin, 2005).

[16] L. V. Keldysh, Sov. Phys. JETP **20**, 1307 (1965).

[17] P. Sprangle, J. R. Peñano, and B. Hafizi, Phys. Rev. E **66**, 046418 (2002).

[18] G. Gibson, T. S. Luk, and C. K. Rhodes, Phys. Rev. A **41**, 5049 (1990).

[19] S. Augst, D. D. Meyerhofer, D. Strickland, and S. L. Chint, J. Opt. Soc. Am. B **8**, 858 (1991).

[20] G. P. Agrawal, *Nonlinear Fiber Optics* (Academic, San Diego, CA, 2007), 4th ed.

[21] W. M. Wood, C. W. Siders, and M. C. Downer, IEEE Trans. Plasma Sci. **21**, 20 (1993).

[22] A. Börzsönyi, Z. Heiner, A. P. Kovács, M. P. Kalashnikov, and K. Osvay, Opt. Express **18**, 25 847 (2010).

[23] W. Chang, A. Nazarkin, J. C. Travers, J. Nold, P. Hölzer, N. Y. Joly, and P. St. J. Russell, Opt. Express **19**, 21 018 (2011).

[24] The ratio between $\tilde{\sigma}'$ and $\tilde{\sigma}$ is the ratio between the pulse energy contributing to the plasma formation and the total energy of the pulse. Full details about computing $\tilde{\sigma}'$ will be reported elsewhere.

[25] E. M. Dianov, A. Ya. Karasik, P. V. Mamyshev, A. M. Prokhorov, V. N. Serkin, M. F. Stel'makh, and A. A. Fomichev, JETP Lett. **41**, 294 (1985).

[26] F. M. Mitschke and L. F. Mollenauer, Opt. Lett. **11**, 659 (1986).

[27] A. G. Bulushev, E. M. Dianov, O. G. Okhotnikov, and V. N. Serkin, JETP Lett. **54**, 619 (1991).

[28] J. K. Lucek and K. J. Blow, Phys. Rev. A **45**, 6666 (1992).

[29] A. V. Husakou and J. Herrmann, Phys. Rev. Lett. **87**, 203901 (2001).

[30] E. A. J. Marcatili and R. A. Schmeltzer, Bell Syst. Tech. J. **43**, 1783 (1964).